Biosensors and Bioelectronics 133 (2019) 223–229

Contents lists available at ScienceDirect

Biosensors and Bioelectronics

journal homepage: www.elsevier.com/locate/bios

A high-sensitivity thermal analysis immunochromatographic sensor based on au nanoparticle-enhanced two-dimensional black phosphorus photothermal-sensing materials

Shijie Li[a], Ying Zhang[a], Wenjun Wen[a], Wei Sheng[a], Junying Wang[c], Shuo Wang[b,*], Junping Wang[a,*]

[a] State Key Laboratory for Food Nutrition and Safety; College of Food Engineering and Biotechnology, Tianjin University of Science and Technology, Tianjin 300457, PR China
[b] Beijing Technology and Business University, Higher Education Garden, Liangxiang, Beijing 100035, PR China
[c] The Biotechnology Research Institute of Chinese Academy of Agricultural Sciences, Beijing 10010, PR China

ARTICLE INFO

Keywords:
Black phosphorus nanosheets
Au nanoparticle-enhanced black phosphorus photothermal sensing probes
Thermal sensing immunochromatographic sensor
Quantitative detection
Enrofloxacin

ABSTRACT

For the first time, a quantitative photothermal-sensing immunochromatographic sensor (PT-ICS) is described using Au nanoparticle-enhanced two-dimensional black phosphorus (BP-Au) as signal component for the photothermal-sensing antibody probe. BP-Au has good photothermal properties at 808 nm, and the photothermal conversion efficiency of the BP-Au nanosheet increased by 12.9% over the black phosphorus nanosheet alone. In addition, the antibody was more easily coupled to this nanosheet due to the good physical adsorption capacity of Au nanoparticles. We used this PT-ICS to detect veterinary antibiotics enrofloxacin (ENR), the photothermal-sensing antibody probe was competitive captured by ENR target and antigen coating on test (T) lines of the sensor. This process was exothermic under an 808 nm laser, and the thermal energy decreased as the ENR in the sample increased. This thermal energy was recorded by an infrared thermal imager or an infrared thermometer, and the concentration of the ENR residues in animal-derived foods was obtained by analyzing the temperature changes in T-lines. Under optimal conditions, the PT-ICS exhibited sensitive and specific detection of ENR from 0.03 μg/L to 10 μg/L with detection limits of 0.023 μg/L. The results agreed well with a commercial enzyme-linked-immunosorbent assay kit. This PT-ICS provided a promising strategy for the detection of ENR residues in animal-derived foods and expected to be used for the detection of other highly sensitive biomacromolecules.

1. Introduction

In the past decade, many single-layer/multi-layer 2D nanomaterials (Zhuang et al., 2015) with various unique physical and chemical properties have been extensively studied including graphene (Tu et al., 2018), transition metal dichalcogenides (TMDs) (Yan et al., 2018), metal or covalent organic frameworks (MOFs or COFs) (Huang et al., 2016a; Simon-Yarza et al., 2018), layered double hydroxides (LDHs) (Sajid and Basheer, 2016), and hexagonal boron nitride (*h*-BN) (Weng et al., 2016). These have broad applications in optoelectronics, electronics, energy storage and conversion, and biomedicine. In addition, black phosphorus nanosheets (BPNSs) (Yi et al., 2017), which were first reported to be stripped from bulk BP in 2014 (Liu et al., 2014), combine the properties of various 2D materials mentioned above and are becoming a promising and extraordinary nanomaterial.

BP is a direct band gap semiconductor that can be directly coupled to light. With a reduction in the number of layers, the band gap can be adjusted to 0.3–1.8 eV (Roldán and Castellanos-Gomez, 2017). This has been used to build a new generation of optoelectronic devices for spectral detection across the entire visible-to-near-infrared region. Black phosphorous is also a natural P-type semiconductor (Dai and Zeng, 2014), and two-dimensional black phosphorus has good catalytic reduction abilities in photocatalysis. Moreover, the unique mechanical, electrical, and thermal anisotropy of black phosphorus gives two-dimensional black phosphorus crystals a variety of excellent properties. BPNSs have large surface-to-volume ratio and excellent photothermal

* Corresponding authors.
E-mail addresses: wangjp@tust.edu.cn (S. Wang), wangjp@tust.edu.cn (J. Wang).

https://doi.org/10.1016/j.bios.2019.03.039
Received 15 January 2019; Received in revised form 15 March 2019; Accepted 18 March 2019
Available online 20 March 2019
0956-5663/

properties, and have made outstanding contributions to disciplines such as bioimaging (Chen et al., 2017), bio-diagnosis, photothermal therapy, drug delivery (Mo et al., 2018; Tao et al., 2017), and biosensing (Zhang et al., 2018).

Importantly, chemical instability not required in most of the above applications can also be used for metal nanoparticle synthesis to the surface of BPNSs to construct biosensors. Peng et al. (2017) decorated Au nanoparticles (AuNPs) on the surface of a few layers of BPNSs to reduce 4-nitrophenol under the synergistic interactions of AuNPs and a BPNSs. Liu et al. (2018) achieved chemo-photothermal tumor therapy and label-free live-cell bioimaging utilizing the extraordinary near-infrared (NIR) photothermal performance and Raman performance of black phosphorus − Au nanoparticle hybrids (BP − Au). These results demonstrate the broader application potential of modified BPNSs.

Immunochromatographic sensors (ICSs) (Huang et al., 2016b) are highly regarded qualitative and semi-quantitative detection tools. They have been widely used in the fields of biomedical diagnostics and food safety detection due to their simple operation, rapid detection, and low cost. In addition, ICSs are an irreplaceable on-site screening tool—they are not dependent on complex instruments. In addition, they are small, portable, and offer visual results in real-time.

In conventional immunoassays using nanomaterials as signal probes, the optical properties of these materials is usually used as the basis for signal output (Ming et al., 2014; Shen et al., 2017), but their excellent photothermal-sensing capabilities have been woefully neglected. The photothermal properties of AuNPs have been described in several previous reports. Qin et al. (2012) re-evaluated the performance of FDA-approved *cryptococcus* antigen immunochromatographic test strips using the thermal-sensing properties of AuNPs. Their results showed that a thermal signal could be used for analysis, and the sensitivity of this strip was increased 32-fold using this innovation. Song et al. (2018) also established a photothermal laser speckle imaging assay to re-evaluate the performance of FDA-approved *cryptococcus* antigen immunochromatographic strips demonstrating signal detection with a sensitivity that is 68-fold higher than colorimetric assays. A thermal signal output mode based on the photothermal performance of a label material requires observations of the temperature change via only an inexpensive laser and an infrared thermometer, and results can be obtained by a simple mathematical conversion without using other expensive instrumentation. Applying this signal output mode to ICSs provides a novel approach for the development of quantitative ICSs. Therefore, a combination of the excellent photothermal performance of BP − Au nanosheets with the portable and rapid detection features of ICS can be used to construct a more sensitive thermal-sensing immunoassay.

Enrofloxacin (ENR) is the world's first animal-specific quinolone which approved by the FDA as a livestock and fish antibacterial agent in 1996 (Nelson, 2004). It has been widely used as an antibiotic in veterinary medicine (Mitchell, 2006). However, the residues of ENR often appear in animal-derived foods causing chronic or acute poisoning, allergic reactions, teratogenic carcinogenesis mutagenic effects, and damage to the human gastrointestinal flora balance (Yu et al., 2014). To regulate the use of ENR and ensure that its residual concentration in animal-derived foods is at an acceptable level, many countries and organizations have established maximum residue limits for ENR in animal-derived foods (Chen et al., 2009; Fernandez et al., 2011).

Thus, we prepared a BP − Au − Ab photothermal-sensing probe by utilizing the good photothermal conversion property and chemical instability of BPNSs and developed a photothermal immunochromatographic sensor (PT-ICS) for a sensitive and quantitative detection ENR. The performance of these PT-ICSs was evaluated with respect to the limit of detection (LOD, IC_{15} value), sensitivity (IC_{50} value), accuracy, and precision. In addition, we verified the sensitivity and reliability of our measurements by detecting animal-derived food samples respectively with PT-ICS and a commercially available ELISA kit.

2. Material and methods

2.1. Materials and reagents

Gold acid chloride trihydrate ($HAuCl_4{\cdot}3H_2O$), sodium citrate, bovine serum albumin (BSA), and ovalbumin (OVA) were purchased from Sigma-Aldrich Co. LLC. (St. Louis, MO, USA). BPNSs were purchased from Nanjing XFNANO Materials Tech Co., Ltd (Nanjing, China). Tris, sucrose, polyvinylpyrrolidone (PVP), poloxamer 18 solution (F68), TritonX-100, SDS-L, and polyethylene glycol (PEG_{200}), were purchased from Sangon Biotech Co., Ltd (Shanghai, China). Enrofloxacin, flumequine, danofloxacin, sparfloxacin, gatifloxacin, fleroxacin, lomefloxacin, difloxacin, sarafloxacin, ciprofloxacin, and norfloxacin were purchased from Dr. Ehrenstorfer GmbH (Augsburg, Germany). A commercial ENR ELISA test kit was purchased from Reagen LLC (Moorestown, NJ, USA). Anti-ENR polyclonal antibody (Ab) was produced in our laboratory. Nitrocellulose (NC) membranes (HF135 with capillary flow 135 s/4 cm) were purchased from the Millipore Corporation (Bedford, MA, USA). Sample pads, conjugate pads, absorbent pads, and polyvinyl chloride (PVC) sheets were purchased from Kinbio Tech Co. (Shanghai, China). The results of PT-ICSs were determined using a FOTRIC 226 s infrared thermal imager (Shanghai FOTRIC Technology Co., China).

2.2. Preparation of a photothermal-sensing probe (black phosphorus-Au nanosheet-antibody conjugate, BP-Au-Ab)

A BP − Au hybrid nanosheet was synthesized according to previous reports with slight modifications (Lee et al., 2016). All synthetic details are provided in the electronic Supplementary material.

A BP-Au-Ab coupling complex was prepared by physical adsorption. Here, 0–5 μL of 27.6 mg/mL K_2CO_3 and 3–5 μL of 0.65 mg/mL ENR-Ab were added to 400 μL of BP-Au, and the mixture was incubated for 1 h at room temperature. Next, 10 μL of a 20% BSA aqueous solution and 5 μL of 10% PEG-20000 were added to the solution, and the mixture was incubated for 30 min at room temperature and then centrifuged at 12,000 rpm for 15 min at 4 °C. The supernatant was discarded, and the precipitate was dissolved in 80 μL of working buffer for use.

2.3. Preparation of enrofloxacin coating antigen (ENR-OVA)

ENR-OVA with a molar ratio of OVA to ENR of 1:25 was synthetized according to the mixed acid anhydride method (Gendloff et al., 1986) with slight modification; full details can be found in the Supplementary material.

2.4. Test procedure

The 100 μL of a standard or sample solution and 2.5 μL of the BP-Au-Ab sensing probe were mixed together and dropped onto the sample pad with visual results being obtained within 10 min by the naked eye. After the test strip had dried, the T-line was irradiated with an 808 nm laser for 30 s, and the results were captured with an infrared thermal imager. The laser spot diameter was 0.37 cm, and the power density was 8.1 mw/mm^2.

3. Results

3.1. Characterization of the BP-Au nanosheets

The preparation method used to create the BP-Au-Ab photothermal-sensing probe is shown in Scheme 1a. The AuNPs were reduced on the surface of the BPNSs utilizing the chemical instability of the BPNSs. Due to the good physical adsorption property of AuNPs, an ENR antibody (Ab) was then coupled to the BP-Au nanosheets to prepare a highly specific photothermal-sensing probe (BP-Au-Ab).

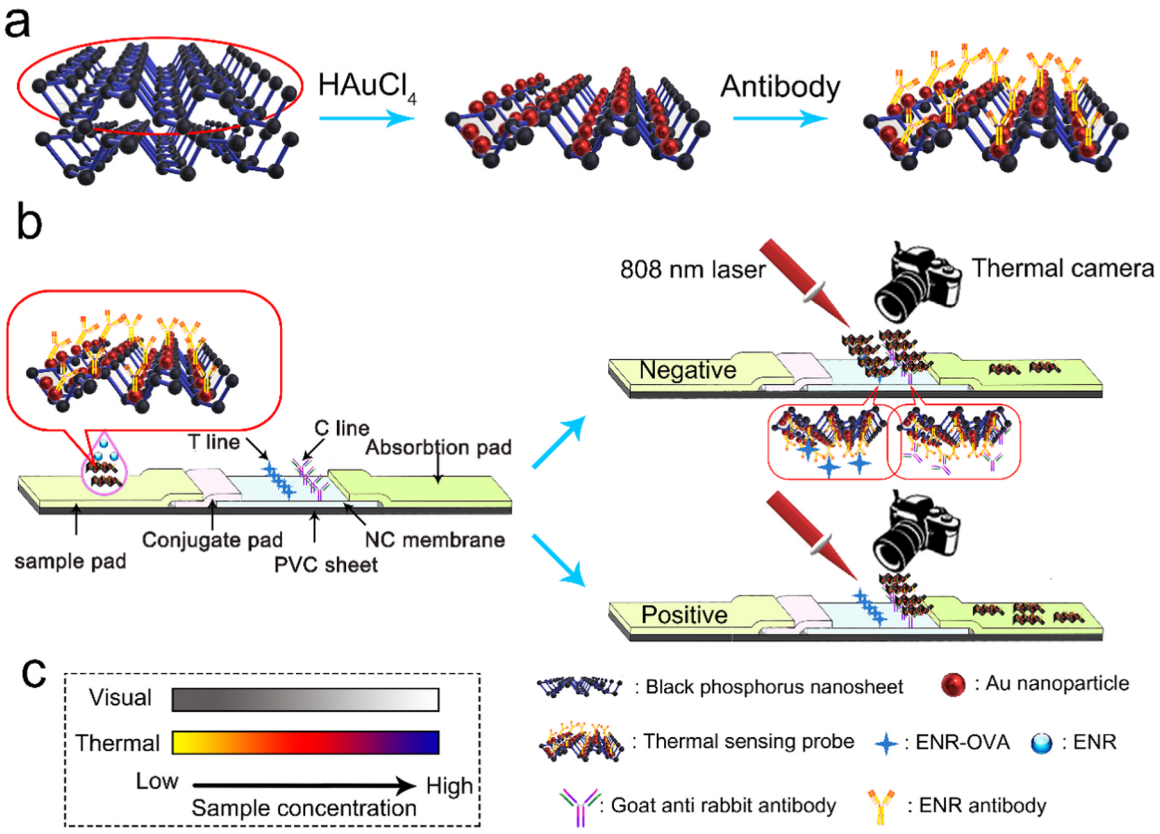

Scheme 1. Schematic of PT-ICSs. (a) Preparation method of the BP-Au-Ab photothermal-sensing probe. (b) Structure and test procedures of PT-ICSs, C-line: control line [anti-rabbit antibody] and T-line: test line [ENR-OVA]. (c) Schematic of comparison of colorimetric results with photothermal results.

$HAuCl_4$ can be reduced onto AuNPs on the surface of BPNSs at room temperature, and the color of this mixture changed from light brown to brown-purple (Fig. 1a and b, Inset). Before reduction, the BPNSs had a relatively uniform and irregular sheet structure (Fig. 1a), and Raman spectroscopy showed that there were three Raman peaks at 360.1 cm^{-1}, 436.8 cm^{-1}, and 465.3 cm^{-1} from the BPNSs corresponding to the A_g^1, B_{2g} and A_g^2 modes, respectively (Guo et al., 2016) (Fig. S1). The amount of $HAuCl_4$ used influenced the amount of AuNP adhered to the surface of the black phosphorus, and the consistency of the particle size distribution thus affected the stability of PT-ICA (please see Supplementary material). Under optimal conditions, AuNPs with a particle size of 14.46 ± 3.21 nm were formed on the surface of the BPNSs after adding 125 μL of 3.9 mg/mL $HAuCl_4$ to the BPNS solution (Fig. 1b and c); the SPR peak of AuNP appeared, and the absorbance at 808 nm is also on the rise (Fig. 1d).

For a photothermal-sensing probe, the photothermal conversion efficiency (η) is an important indicator to evaluate the probe quality. Thus, the η of BPNSs and BP-Au nanosheets was evaluated as follows (Ren et al., 2015):

$$\eta = \frac{hA(T_{max} - T_{sur}) - hA(T_{max,water} - T_{sur,water})}{I(1-10^{-A_\lambda})} \times 100\%. \quad (1)$$

Here, h is the heat transfer coefficient, A is the surface area of the container, A_λ is the absorbance of materials at a wavelength of 808 nm in an aqueous solution, T_{max} is the highest solution temperature, and the T_{sur} is the ambient temperature of the surrounding environment. Specific calculation details are listed in the Supplementary material. The η of the BPNSs was 23.2%, and the η of the BP-Au nanosheets was 36.1%.

The optical images, photothermal images and temperature trends of a series of concentrations of BP and BP-Au dripped onto NC films was evaluated by the results of the Fig. 2. The slight difference between the same concentration of BP and BP-Au cannot be seen by optical imaging, and signals can be captured by an optical camera only when the concentration is increased to 50 μg/mL (Fig. 2a). However, the infrared thermal imager converted the grayscale image into a color image by a thermal signal, the change in the concentration of the material can be more clearly distinguished on the image (Fig. 2b). And due to the higher photothermal conversion efficiency, the range of colors of BP-Au nanosheet that can be captured is wider (12.5–200 μg/mL for BP-Au, however 100–200 μg/mL for BPNSs). In addition, the temperature trends of BPNSs and BP-Au was analyzed. Obviously, when the same concentration is increased or decreased, the temperature change rate of gold nanoparticles is larger, which provides favorable conditions for distinguishing small concentration changes of analyte. Therefore, materials with high photothermal conversion rate have greater advantages in detecting low concentration or trace concentration change sample.

3.2. Sensitivity

For PT-ICSs, the absorption and heat release of the sensor carrier, the intensity of the infrared light illumination, and the spot area play decisive roles in the successful construction of sensitive and stable sensors. Therefore, we measured bare NC membrane, a PVC sheet, a NC membrane stuck on a PVC sheet, the T-line for strip detection of an ENR-free solution, and the T-line for strip detection of a 1 μg/L ENR solution. All samples were irradiated with an 808 nm laser at different power densities (7.55–9.70 mW/mm^2) and over different spot areas. A full analysis of these parameters is in the Supplementary material.

Under the optimal conditions, an infrared laser with an 8.08 mW/mm^2 power density and a 3.7 mm spot area was used as a laser source for the PT-ICSs. In addition, the ionic strength of the coupling buffer, the amount of antibody used during probe preparation, and the amount of coating antigen on T-lines are other key factors that influence the

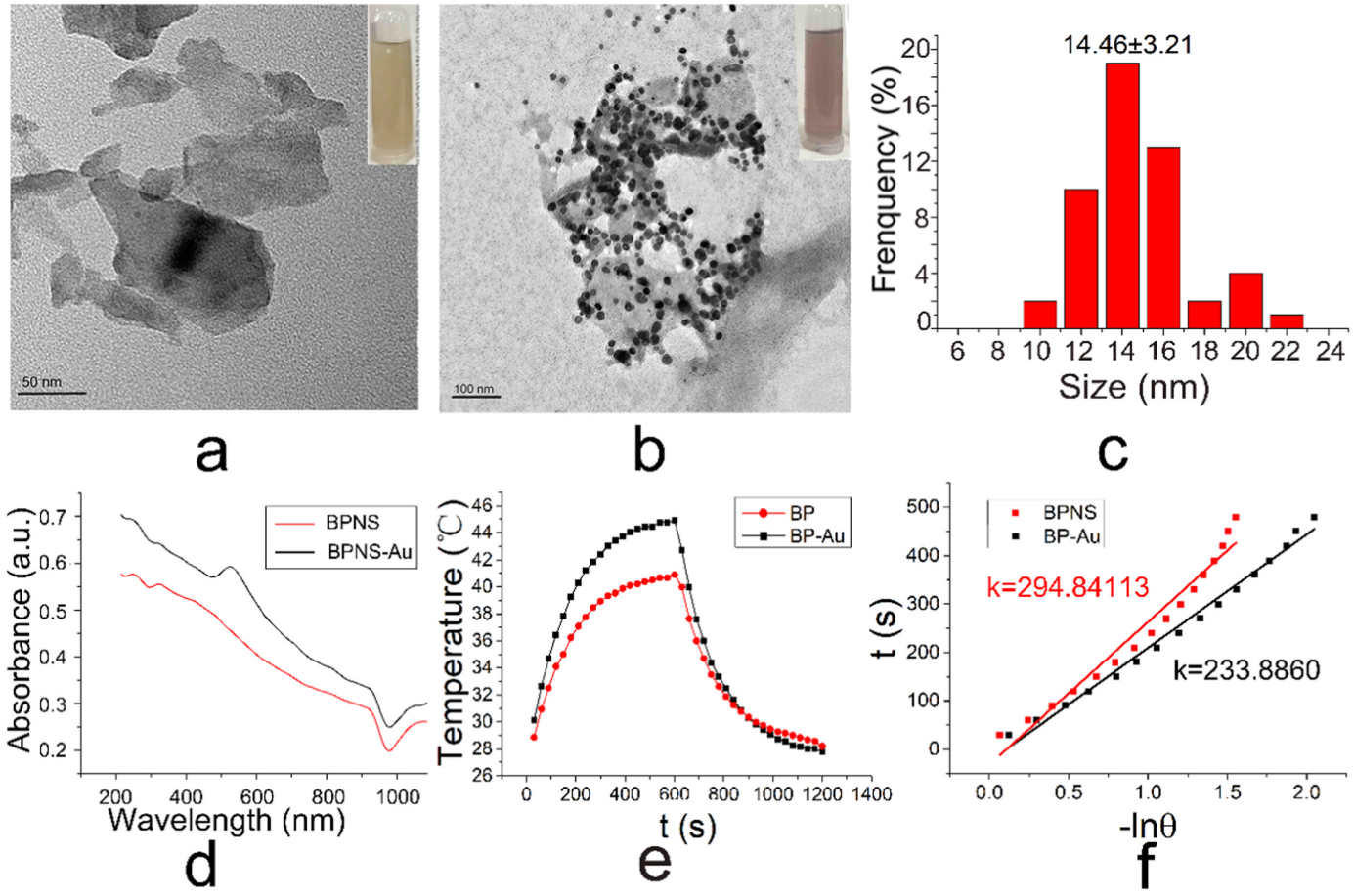

Fig. 1. Characterization of BPNSs and BP-Au nanosheets. TEM images of (a) PBNSs and (b) BP-Au nanosheet with 125 μL of 3.9 mg/mL $HAuCl_4$ added; (c) Au particle size statistics of BP-Au nanosheets; (d) UV–Vis–NIR spectroscopy of PBNSs and BP-Au nanosheets; (e) temperature response to 808 nm laser (1 W cm^{-2}) irradiation on and off of PBNSs as well as a BP-Au nanosheet (200 μg/mL) over a period of 1200 s; (f) Linear time data versus − ln θ obtained from the cooling period of Fig. 2e.

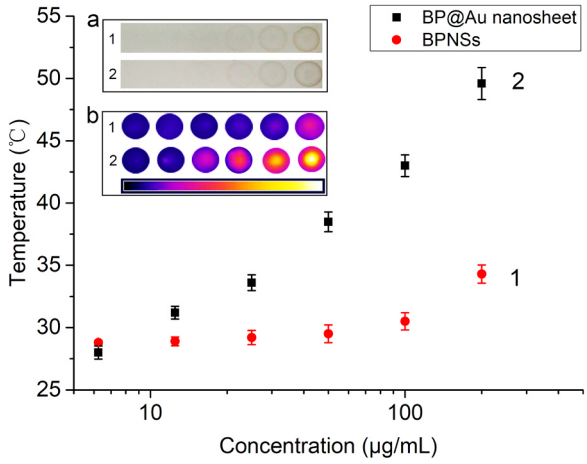

Fig. 2. Photothermal response of BPNS (1) and BP-Au nanosheet (2) spotted on NC membranes at various concentrations. Inset-a: Visual image; and Inset-b: Photothermal image.

sensitivity of PT-ICSs. After optimizing, (Fig. S5 and Table S1), a sensitive PT-ICS was successfully established. The detection principle is explained in more detail in the Supplementary material.

The results of the PT-ICS detection of ENR in PBS buffer is shown in Fig. 3. The imaging data for PT-ICSs detecting 0, 0.005, 0.01, 0.03, 0.1, 0.5, 1, 3, 5, 8, 10, and 15 μg/L ENR are shown in Fig. 3a. The visual data in Fig. 3a (1) shows the brown-purple color of the T-line gradually became shadowed when the concentration of ENR was at 0.5 μg/L. It disappeared at 5 μg/L ENR. Thus, the LOD of the visual inspected PT-ICS was 0.5 μg/L, and the cut-off value was 5 ng/L. For thermal inspection, the imaging results of the infrared thermal imager are shown in Fig. 3a (2), and a logarithmic standard curve of the inhibition ratio of temperature variation on the T-line is shown in Fig. 3b. As the concentration of ENR increased, the image point captured by the thermal imager gradually changed from bright yellow to purple indicating that the temperature gradually decreased. In Fig. 3a (1), the color of the T-line was hardly visible when the concentration of ENR was over 5 μg/L, and an accurate concentration of ENR could not be judged by visual inspection. However, the color of the T-line in Fig. Fig. 3a (2) could still be detected by the infrared imager when the concentration of ENR reached 10 μg/L, the small amount of BPNS-Au remaining on the T-line could still absorb energy and release heat. Therefore, PT-ICSs can detect a wider range of concentrations than visual inspection. A logarithmic standard curve was generated to facilitate a quantitative analysis of ENR concentration. The LOD (IC_{15}) of the thermally inspected PT-ICSs according to the logarithmic standard curve was 0.023 μg/L, the sensitivity (IC_{50}) was 0.57 μg/L (R^2 = 0.996), and the linear range was from 0.03 to 10 μg L^{-1} (R^2 = 0.992).

3.3. Specificity

Ten kinds of quinolones were chosen to evaluate the specificity of the PT-ICS (Fig. S6). The inhibition ratios were 16.07% and 83.75% when the concentration of ENR was 0.03 and 5 μg/L, respectively. The inhibition ratios were lower than 10% when the concentrations of

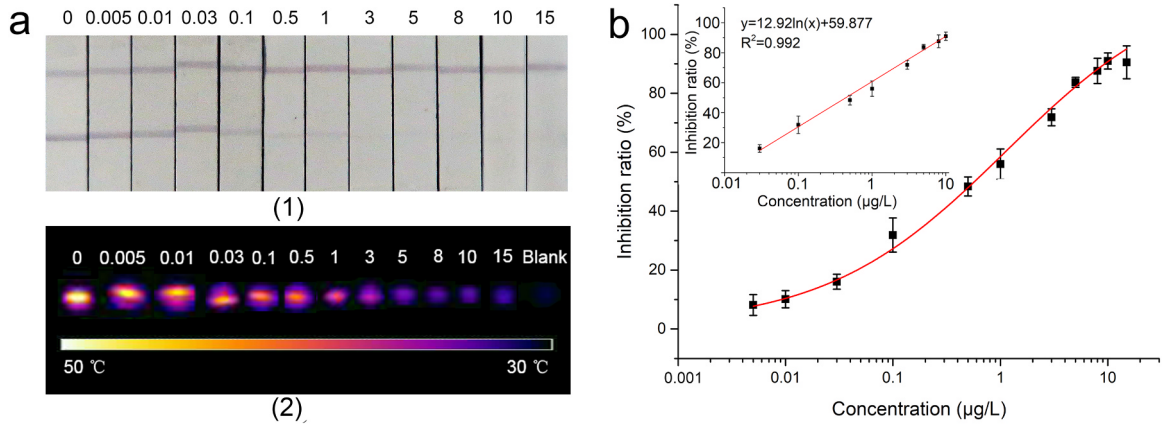

Fig. 3. Imaging results (a) 0, 0.005, 0.01, 0.03, 0.1, 0.5, 1, 3, 5, 8, 10, and 15 μg/L ENR in PBS buffer (0.01 mol/L, pH 7.4) by optical camera (1) and thermal imager (2). Imaging (b): inhibition rate curve; Inset: linear range of the detection results.

flumequine, danofloxacin, sparfloxacin, gatifloxacin, fleroxacin, lomefloxacin, difloxacin, sarafloxacin, ciprofloxacin, or norfloxacin were 100 μg/L. These results indicated that the PT-ICS had high specificity for the analysis of ENR.

3.4. Sample analysis

The matrix components and organic reagents in a sample extract are important factors for interfering with the specific binding of antigen to antibody and thus affecting the sensitivity of our detection method. Thus, a series of concentrations of ENR solution was constructed using diluted chicken tissue extracts and detected using a PT-ICS to eliminate any potential matrix effects (Please see Supplementary material). Fig. S7 shows that the detection results of ENR in 15-fold diluted tissue extract solution was basically consistent with the detection results of ENR in PBS buffer. Here, the matrix component and the organic reagents (5.3%) in the extract did not significantly interfere with the specific binding of antigen and antibody. Therefore, the sample extract was diluted 15-fold and was used for detection in further recovery analyses.

Animal-derived food samples were determined to be ENR free using a commercial ELISA test kit from REAGEN. ENR was introduced to samples to give final concentrations of 0, 0.5, 5.0, 25.0, and 50.0 μg/kg, respectively, and the samples were then measured by PT-ICS (Table 1). The ENR values measured by the intra-assay were between 72.6% and 126.2%, the coefficients of variation (CV) were 2.64–15.36%, and the recoveries between batches were between 71.4% and 126.4% with coefficients of variation between 7.04% and 19.28%.

A commercial ELISA test kit was then used to verify the accuracy and practicality of our method (Table 1). Our results agreed well with the results obtained using the ELISA kit. This showed that this method had good practicality. Compared with a traditional ELISA method, our method is simple, sensitive, fast, and convenient. It can also be a visual semi-quantitative tool. Additionally, it can be used as a thermosensitive quantitative tool for the detection of ENR in animal-derived foods.

4. Discussion

BP-Au nanosheets with excellent near-infrared photothermal properties were proposed as photothermal-sensing probes in immunochromatographic detection of trace amounts of small-molecule contaminants for the first time. BP-Au nanosheets increased the photothermal conversion efficiency by 12.9% over conventional BPNSs at 808 nm laser illumination, and AuNPs on the surface of a BP-Au nanosheet provide good physical adsorption sites for an antibody, so that BP-Au nanosheet was successfully used as probe component and the step of photothermal probe preparation was simplified.

The thermal signal output mode based on the photothermal performance of BP-Au nanosheet had higher sensitivity and a wider detection range than the visual signal observed by the naked eye. First, both the visual analysis and the photothermal analysis can analyze detection results by imaging. But for the visual analysis, we can only analyze detection results by the imaging signal, and for the trace concentration analyte, it is difficult for the naked eye to make a clear resolution. The photothermal analysis can transform the gray level signal which cannot be sensitively distinguished by the naked eye into the color signal which is more sensitive to the naked eye, so as to enhance the resolution of the slightly changed image, and regardless of the high or low analyte concentration, the color signal can be more clearly resolved. In addition, photothermal analysis can record temperature changes as analytical data, which is more intuitive and almost free of background interference than image analysis.

However, the stability of the photothermal sensing probe cannot be compared with other photothermal materials (Gao et al., 2019; Wang et al., 2019). but the possibility of applying these materials to immunochromatographic assays has not been explored. In addition, the particle size of the obtained nanosheet varies due to the restriction of the peeling condition of the black phosphorus nanosheet. In the literature, black phosphorus nanosheets or black phosphorus quantum dots are embedded via a polymer material such as PLGA. This ensures the relative uniformity of the nanospheres and improves the material's stability (Shao et al., 2016). This also expected for further improvements in the stability of PT-ICA.

Among the immunoassays developed in recent years, a variety of materials have been introduced as signal probes (Table 2). However, these optical signal-based analysis assays have limitations in terms of sensitivity or detection range. An immunoassay with a thermal signal output overcomes the shortcomings of poor resolution and background interference of colorimetric signals. It increases the sensitivity and improves the detection range of the method. Quantitative detection of trace contaminants can be achieved with inexpensive infrared thermometers without the need for sophisticated signal processing software.

5. Conclusion

AuNPs synthesized on the surface of a BPNS improved the photothermal conversion ability of the BP-Au photothermal sensing probe and provided sufficient adsorption sites for antibody coupling. We developed an immunosensor utilized the excellent photothermal sensing probe and realized a highly sensitive and quantitative detection of ENR from 0.03–10 μg/L with detection limit of 0.023 μg/L. The recoveries of ENR in animal derived food samples was at levels of 0.5–50 μg/kg ranged from 72.6% to 126.2% with coefficients of variation of

Table 1
Recoveries of ENR from spiked samples via PT-ICA (n = 3).

Sample	Add Conc. (μg/kg (μg/L))	Thermal-LFIA						Visual-ICA	ELISA kit
		Intra-assay[a]			Inter-assay[b]				
		(Average ± SD) (μg/kg (μg/L))	Recovery rate (%)	CV (%)	(Average ± SD) (μg/kg (μg/L))	Recovery rate (%)	CV (%)		(Average ± SD) (μg/kg (μg/L))
Chicken	0.0	ND[c]			ND			-[d],-,-	ND
	0.5	0.55 ± 0.07	107.1	13.45	0.63 ± 0.09	126.4	13.76	-,-,-	ND
	5.0	5.10 ± 0.54	102.0	10.53	5.65 ± 0.86	113.0	15.20	-,-,-	4.82 ± 0.147
	25.0	22.25 ± 2.60	89.0	11.82	21.47 ± 2.28	85.8	10.62	-,-,-	22.70 ± 1.33
	50.0	47.14 ± 3.18	94.3	6.75	47.20 ± 4.86	94.4	10.29	+,+,+	45.98 ± 5.66
Egg	0.0	ND			ND			-,-,-	ND
	0.5	0.43 ± 0.04	85.6	9.11	0.36 ± 0.04	71.4	9.78	-,-,-	ND
	5.0	4.75 ± 0.73	95.2	15.36	4.30 ± 0.72	85.9	16.63	-,-,-	4.94 ± 0.56
	25.0	22.67 ± 1.29	103.5	5.69	22.52 ± 3.31	90.1	14.70	-,-,-	23.7 ± 2.19
	50.0	48.65 ± 6.22	97.3	12.78	52.67 ± 7.01	105.3	13.30	+,+,+	47.39 ± 3.65
Pork	0.0	ND			ND			-,-,-	ND
	0.5	0.36 ± 0.05	72.6	13.49	0.39 ± 0.04	78.2	10.99	-,-,-	ND
	5.0	4.33 ± 0.42	86.6	9.69	4.72 ± 0.91	94.4	19.28	-,-,-	4.54 ± 0.62
	25.0	24.27 ± 0.64	94.6	2.64	19.42 ± 2.65	77.6	13.64	-,-,-	24.40 ± 2.39
	50.0	41.29 ± 5.31	82.6	12.86	43.53 ± 6.31	87.1	14.49	+,+,+	52.66 ± 3.01
Beef	0.0	ND			ND			-,-,-	ND
	0.5	0.63 ± 0.09	126.2	13.47	0.61 ± 0.04	122.2	7.04	-,-,-	ND
	5.0	4.17 ± 0.45	83.4	10.79	4.91 ± 0.64	98.1	13.03	-,-,-	4.73 ± 0.34
	25.0	27.43 ± 3.24	109.8	11.81	26.59 ± 4.32	106.4	16.24	-,-,-	23.70 ± 0.618
	50.0	51.32 ± 3.12	102.6	6.08	52.75 ± 8.85	105.5	9.74	+,+,+	46.12 ± 3.35
Crucian1	0.0	ND			ND			-,-,-	ND
	0.5	0.41 ± 0.03	81.0	8.15	0.38 ± 0.05	75.8	13.98	-,-,-	ND
	5.0	4.35 ± 0.38	87.0	8.74	6.32 ± 0.81	126.4	12.82	-,-,-	5.24 ± 0.48
	25.0	27.40 ± 3.76	109.6	13.72	25.52 ± 1.83	102.1	7.17	-,-,-	23.06 ± 1.38
	50.0	46.15 ± 3.94	92.3	8.54	48.45 ± 4.87	96.9	10.05	+,+,+	43.45 ± 4.69

[a] Intra-assay variations were determined by three replicates on a single day.
[b] Inter-assay variations were determined by a single test on three different days.
[c] ND: Negative detection results.
[d] −: Negative visual result. +: Positive visual result.

Table 2
An overview on reported immunoassays of for determination of ENR.

Methods	Materials	LODs (μg/L)	Detection range	Ref.
Fluoroimmunoassay	Quantum dots	2.5	1–100	(Chen et al., 2009)
Chemiluminescence immunoassay	Phosphatase-adamantane	0.24	0.35–1	(Yu et al., 2012)
Chemiluminescence immunoassay	Horseradish peroxidase-luminol-H_2O_2	0.003	0.35–1	(Yu et al., 2014)
Barcoded-immunochromatographic	Au nanoparticle	8	—	(Yang et al., 2017)
Immunochromatographic	Au nanoparticle	0.089	—	(Wu et al., 2016)
Immunochromatographic	$Ru(phen)_3^{2+}$-Doped Silica Nanoparticles	0.02	0.025–3.5	(Huang et al., 2013)
Immunochromatographic	Quantum dots	1 (visual)	—	(Sheng et al., 2017)
Immunochromatographic	Au nanoparticle	0.25	0.25–2.5	(Peng et al., 2016)
Immunochromatographic	PB@Au nanosheet	0.023	0.03–10	This work

2.64–15.36%. However, further improvements in the stability and uniformity of the probe could further increase the sensitivity—this is part of our future work. The PT-ICS lays the foundation for the development of other biomacromolecules detection sensors based on the principle of sandwich detection. The application of PT-ICS in clinical diagnosis should be continued in follow-up studies.

Acknowledgment

This work was supported by “The National Key R&D Program of China” (No. 2016YFD0401202); and the Special Project of Tianjin Innovation Platform (No. 17PTGCCX00230).

Funding

This work was supported by Tianjin University of Science and Technology 2018 Excellent Doctoral Dissertation Innovation Fund Project [grant no. 201803].

We thank LetPub (www.letpub.com) for its linguistic assistance during the preparation of this manuscript.

Declaration of interest statement

In this work, the Au nanoparticle (AuNP)-enhanced black phosphorus nanosheet (BPNS) was explored as a photothermal sensing detection element for the establishment of immunochromatographic analysis methods, and a novel method for quantitative detection of veterinary antibiotic enrofloxacin (ENR) in animal-derived foods was developed. Using chemical instability of BPNS, $HAuCl_4$ was reduced as Au nanoparticle on the surface of BPNS in situ. After reduction, the near-infrared absorption of the BPNS was enhanced and the photothermal conversion efficiency improved (increased by 12.9% over a simple BPNS under 808 nm laser illumination,). Additionally, due to the good physical adsorption capacity of the AuNPs, the ENR antibody was successfully adsorbed, and a photothermal sensing immuno-probe was prepared.

Since the black phosphorus nanosheet has good dispersibility in water, the probe can be chromatographed on the NC membrane by capillary force. ENR in the sample competed with the coating antigen at the T line on the NC membrane to bind to the antibody adsorbed on the surface of the probe. Under the illumination of 808 nm laser, the probe captured by the antigen at the T line undergone photothermal conversion, and the temperature change was captured by an infrared imager or an infrared thermometer. Since the measured temperature decreases as the amount of ENR in the sample increases, the quantitative analysis of ENR was achieved by a simple calculation of the change in temperature at the T line. This method had good linear range for the detection of ENR at 0.03–10 μg/L in PBS buffer and 0.45–150 μg/kg in animal-derived food samples.

Compared to other quantitative analysis methods, this method eliminates the need for complex signal capture and signal conversion instruments and complex data analysis systems, quantitative analysis can be achieved only by recording changes in temperature through an infrared thermometer. At the same time, compared with the visual analysis method, the application of the photothermal sensing analysis method can further improve the sensitivity and widen the detection range. This method is expected to be used for the establishment of quantitative detection methods for macromolecular biomarkers to further improve the sensitivity of disease diagnosis methods.

Appendix A. Supplementary material

Supplementary data associated with this article can be found in the online version at doi:10.1016/j.bios.2019.03.039.

References

Chen, J., Xu, F., Jiang, H., Hou, Y., Rao, Q., Guo, P., Ding, S., 2009. Food Chem. 113 (4), 1197–1201.

Chen, W., Ouyang, J., Liu, H., Chen, M., Zeng, K., Sheng, J., Liu, Z., Han, Y., Wang, L., Li, J., Deng, L., Liu, Y.N., Guo, S., 2017. Adv. Mater. 29 (5).

Dai, J., Zeng, X.C., 2014. J. Phys. Chem. Lett. 5 (7), 1289–1293.

Fernandez, F., Pinacho, D.G., Sanchez-Baeza, F., Marco, M.P., 2011. J. Agric. Food Chem. 59 (9), 5036–5043.

Gao, H., Chen, Y., Li, H., Zhang, F., Tian, G., 2019. Chem. Eng. J. 363, 247–258.

Gendloff, E.H., Casale, W.L., Ram, B.P., Tai, J.H., Pestka, J.J., Hart, L.P., 1986. J. Immunol. Methods 92 (1), 15.

Guo, Z., Zhang, H., Lu, S., Wang, Z., Tang, S., Shao, J., Sun, Z., Xie, H., Wang, H., Yu, X.F., 2016. Adv. Funct. Mater. 25 (45), 6996–7002.

Huang, N., Wang, P., Jiang, D., 2016a. Nat. Rev. Mater. 1 (10).

Huang, X., Aguilar, Z.P., Li, H., Lai, W., Wei, H., Xu, H., Xiong, Y., 2013. Anal. Chem. 85 (10), 5120–5128.

Huang, X., Aguilar, Z.P., Xu, H., Lai, W., Xiong, Y., 2016b. Biosens. Bioelectron. 75, 166–180.

Lee, H.U., Park, S.Y., Lee, S.C., Choi, S., Seo, S., Kim, H., Won, J., Choi, K., Kang, K.S., Park, H.G., Kim, H.S., An, H.R., Jeong, K.H., Lee, Y.C., Lee, J., 2016. Small 12 (2), 214–219.

Liu, H., Neal, A.T., Zhu, Z., Luo, Z., Xu, X., Tománek, D., Ye, P.D., 2014. ACS Nano 8 (4), 4033–4041.

Liu, Z., Haolin, C., Jia, Y., Zhang, W., Zhao, H., Fan, W., Zhang, W., Zhong, H., Ni, Y., Guo, Z., 2018. Nanoscale 10, 18795–18804.

Ming, C., Chen, X., Xu, P., Pen, J., Zhu, X., Zhu, D., 2014. J. Exot. Pet. Med. 15 (1), 66–69.

Mo, J., Xie, Q., Wei, W., Zhao, J., 2018. Nat. Commun. 9 (1), 2480.

Nelson, R., 2004. Lancet Infect. Dis. 4 (5), 258.

Peng, J., Lai, Y., Chen, Y., Xu, J., Sun, L., Weng, J., 2017. Small 13 (15), 1603589.

Peng, J., Liu, L., Xu, L., Song, S., Kuang, H., Cui, G., Xu, C., 2016. Nano Res. 10 (1), 108–120.

Qin, Z., Chan, W.C., Boulware, D.R., Akkin, T., Butler, E.K., Bischof, J.C., 2012. Angew. Chem. 51 (18), 4358–4361.

Ren, W., Yan, Y., Zeng, L., Shi, Z., Gong, A., Schaaf, P., Wang, D., Zhao, J., Zou, B., Yu, H., 2015. Adv. Healthc. Mater. 4 (10), 1526–1536.

Roldán, R., Castellanos-Gomez, A., 2017. Nat. Photonics 11 (7), 407–409.

Sajid, M., Basheer, C., 2016. TrAC Trends Anal. Chem. 75, 174–182.

Shao, J., Xie, H., Huang, H., Li, Z., Sun, Z., Xu, Y., Xiao, Q., Yu, X.F., Zhao, Y., Zhang, H., Wang, H., Chu, P.K., 2016. Nat. Commun. 7, 12967.

Shen, H., Zhang, S., Fu, Q., Xiao, W., Wang, S., Yu, S., Xiao, M., Bian, H., Tang, Y., 2017. Food Control 81, 101–106.

Sheng, W., Li, S., Liu, Y., Wang, J., Zhang, Y., Wang, S., 2017. Microchim. Acta 184 (11), 4313–4321.

Simon-Yarza, T., Mielcarek, A., Couvreur, P., Serre, C., 2018. Adv. Mater. 30 (37), e1707365.

Song, S., Choi, S., Ryu, S., Kim, S., Kim, T., Shin, J., Jung, H.I., Joo, C., 2018. Biosens. Bioelectron. 117, 385–391.

Tao, W., Zhu, X., Yu, X., Zeng, X., Xiao, Q., Zhang, X., Ji, X., Wang, X., Shi, J., Zhang, H., Mei, L., 2017. Adv. Mater. 29 (1).

Tu, Z., Guday, G., Adeli, M., Haag, R., 2018. Adv. Mater. e1706709.

Wang, Y., Zhao, J., Chen, Z., Zhang, F., Guo, W., Lin, H., Qu, F., 2019. Appl. Catal. B: Environ. 244, 76–86.

Weng, Q., Wang, X., Wang, X., Bando, Y., Golberg, D., 2016. Chem. Soc. Rev. 45 (14), 3989–4012.

Wu, Y., Guo, S., Dong, Q., Song, Y., 2016. Food Anal. Methods 9 (10), 2807–2813.

Yan, C., Gong, C., Wangyang, P., Chu, J., Hu, K., Li, C., Wang, X., Du, X., Zhai, T., Li, Y., Xiong, J., 2018. Adv. Funct. Mater. 28 (39), 1803305.

Yang, M., Zhang, W., Zheng, W., Cao, F., Jiang, X., 2017. Lab Chip 17 (22).

Yi, Y., Yu, X.-F., Zhou, W., Wang, J., Chu, P.K., 2017. Mater. Sci. Eng.: R: Rep. 120, 1–33.

Yu, F., Wu, Y., Yu, S., Zhang, H., Zhang, H., Qu, L., Harrington, Pd.B., 2012. Spectrochim. Acta Part A: Mol. Biomol. Spectrosc. 93, 164–168.

Yu, F., Yu, S., Yu, L., Li, Y., Wu, Y., Zhang, H., Qu, L., Harrington, Pd.B., 2014. Food Chem. 149, 71–75.

Zhang, D., Lin, X., Lan, S., Sun, H., Wang, X., Liu, X., Zhang, Y., Zeng, Y., 2018. Part. Part. Syst. Charact. 35 (4), 1800010.

Zhuang, X., Mai, Y., Wu, D., Zhang, F., Feng, X., 2015. Adv. Mater. 27 (3), 403–427.